NANOSYSTEMS:
PHYSICS, CHEMISTRY, MATHEMATICS

Original article

Kondrat'eva O.N., et al. *Nanosystems: Phys. Chem. Math.*, 2025, **16** (6), 829–836.
http://nanojournal.ifmo.ru
DOI 10.17586/2220-8054-2025-16-6-829-836

Physico-mechanical properties and radiation tolerance of magnesium-indium ferrite synthesized by the polymer-nitrate method

Olga N. Kondrat'eva[1,a], Maria N. Smirnova[1,b], Galina E. Nikiforova[1,c], Alexey D. Yapryntsev[1,d], Maria S. Dranik[2,e], Valery A. Ketsko[1,f]

[1]Kurnakov Institute of General and Inorganic Chemistry of the Russian Academy of Sciences, Moscow, Russia
[2]Frumkin Institute of Physical Chemistry and Electrochemistry of the Russian Academy of Sciences, Moscow, Russia

[a]ol.kondratieva@gmail.com, [b]smirnovamn@igic.ras.ru, [c]gen@igic.ras.ru, [d]yaprynsev@yandex.ru, [e]m.dranik@yandex.ru, [f]ketsko@igic.ras.ru

Corresponding author: Olga N. Kondrat'eva, ol.kondratieva@gmail.com

PACS 81.20.Ev, 81.07.Wx, 62.20.Qp, 78.20.-e

ABSTRACT The paper discusses the features of polymer-nitrate synthesis of fine $MgFeInO_4$ particles and presents experimental study results of the physico-mechanical properties of ceramics produced on their basis. According to powder XRD data, a single-phase ferrite-spinel powder can be obtained only as a result of high-temperature treatment of an X-ray amorphous precursor prepared by thermal decomposition of a mixture of polyvinyl alcohol and metal nitrates. Ceramics produced using submicron $MgFeInO_4$ particles have a density close to the theoretical one. The results of microhardness measurements using the Vickers method showed that the resulting material has high hardness. The band gap energy of $MgFeInO_4$ was determined from the DRS data. Based on the crystallographic and electrophysical characteristics of the synthesized material, its resistance to radiation-induced structural changes was predicted.

KEYWORDS mixed ferrites, cubic crystal structure, fine powders, ceramics, Vickers microhardness, band gap energy, radiation tolerance

ACKNOWLEDGEMENTS This study was performed within the ARIADNA Collaboration operating under the NICA facility as a part of State Assignment "Solving topical problems with NICA charged particle beams" (ref. # 124110600054-0). The measurements were performed using the equipment of the JRC PMR IGIC RAS. The microhardness studies were carried out using the equipment of the CKP FMI IPCE RAS.

FOR CITATION Kondrat'eva O.N., Smirnova M.N., Nikiforova G.E., Yapryntsev A.D., Dranik M.S., Ketsko V.A. Physico-mechanical properties and radiation tolerance of magnesium-indium ferrite synthesized by the polymer-nitrate method. *Nanosystems: Phys. Chem. Math.*, 2025, **16** (6), 829–836.

1. Introduction

The creation of new types of radiation-resistant functional materials suitable for long-term and trouble-free operation under the influence of various sources of ionizing radiation is an important scientific and practical problem. Its solution will create new opportunities for research and development in the field of nuclear energy and medicine, radiation control, and storage of radioactive waste [1–3]. Many years of intensive research [4–6] have shown refractory oxides with a cubic crystal lattice of the spinel type to be one of the most resistant materials to various types of radiation. Materials based on aluminum-magnesium spinel $MgAl_2O_4$ have shown high potential for use in nuclear fission reactors [7,8], as well as inert matrices for transmutation of actinides [7,9,10] and optically transparent windows for reactor components [11]. In addition, it was noted in [12–14] that ferrite-spinels are highly promising for practical application in irradiation environments. Meillon *et al.* [14] established that magnetite (Fe_3O_4) is extremely resistant to fast neutron irradiation with an energy of 0.1 MeV and a fluence of 2×10^{20} neutrons/cm^2, which is equivalent to the radiation conditions near a nuclear reactor.

According to Sickafus *et al.* [15], the excellent radiation tolerance of spinels compared to other materials is due to the complexity of their chemical composition and the ability to cationic disorder. Therefore, the enhancement of their radiation damage resistance is possible due to the complication of the chemical composition (e.g., by polycationic doping) and/or varying the degree of inversion. The cation distribution over tetrahedral and octahedral sublattices of materials with the spinel structure largely depends on the method of their preparation [16, 17]. Moreover, the degree of inversion in microcrystalline samples may differ from their nanoscale counterparts [17]. On the other hand, the size of the powder particles affects the mechanical properties of the materials obtained from them. As it was noted in [18], the strength of ceramics made from ultrafine powders is higher than that of those produced using standard ceramic technology. Moreover,

the large fraction of the grain boundaries can serve as an effective sink of point defects formed during irradiation [19, 20]. This additionally enables creating both new and improved materials for radiation shields and screens, which are today widely in demand in medicine and the nuclear industry [21]. Satalkar *et al.* [22] reported on the high potential of using nanoscale ferrite-spinels $Mn_{1-x}Zn_xFe_2O_4$ ($x = 0$; 0.5; 1) as part of inexpensive lightweight shields designed to protect against radiation near nuclear facilities. Moreover, the mixed ferrite-spinel composition $Mn_{0.5}Zn_{0.5}Fe_2O_4$ was least susceptible to radiation swelling.

According to the literature review, the interest in studying the effect of various irradiation conditions on the structure and structure-sensitive properties of nanoscale ferrite-spinels has been shown to grow [23–28]. Nevertheless, data on the study of the radiation damage resistance of mixed magnesium-indium ferrites has not been found. In this regard, as a starting point for the research work, it is of interest to synthesize and characterize highly dispersed materials based on $MgFe_{2-x}In_xO_4$, in which half of the iron cations are replaced by indium cations. To date, the main approach to produce mixed $MgFe_{2-x}In_xO_4$ ferrite-spinels is the solid-phase method [29–31]. Naik *et al.* [32] attempted low-temperature synthesis of $MgFe_{2-x}In_xO_4$ ($x = 0 - 0.16$) nanoparticles, however, samples with a substitution degree of $x = 0.16$ contained an admixture of α-Fe_2O_3. In this paper, the features of polymer-nitrate synthesis of fine $MgFe_{2-x}In_xO_4$ particles with a high indium content ($x = 0.5$) are described for the first time, as well as the results of measuring microhardness and assessing radiation tolerance of ceramic materials made on their basis are presented.

2. Experimental part

2.1. Synthesis of powder and ceramics of $MgFeInO_4$

Single-phase $MgFeInO_4$ powder was obtained by the polymer-nitrate method. Powders of metallic magnesium (ω(Mg) = 99.95 wt. %, National State Standard GOST 804-93) and carbonyl iron (ultra-high purity 13-2, TS 6-09-05808009-262-92), indium (grade In0, ω(In) = 99.998 wt. %, National State Standard GOST 10297-94), polyvinyl alcohol (PVA, grade 20/1, National State Standard GOST 10779-78) and nitric acid (ultra-high purity 18-4, National State Standard GOST 11125-84) were used as starting materials. The magnesium, indium, and carbonyl iron samples were dissolved in nitric acid previously diluted with distilled water ($V(H_2O) : V(HNO_3) = 1 : 3$). Freshly prepared solutions of $Mg(NO_3)_2$, $Fe(NO_3)_3$, and $In(NO_3)_3$ were mixed in an evaporating bowl in a ratio of 1 :1 : 1, and then heated on a heating plate and kept at 90 °C. A stoichiometric amount of polymer was added to the heated solution mixture and continued to evaporate with constant stirring. Heating was stopped after obtaining a fine red-brown powder. The solid-phase synthesis products formed (hereinafter referred to as the precursor powder) were cooled, ground in a mortar, and then annealed in a muffle furnace. To study the effect of the annealing temperature on the phase composition, the precursor powder was heated to 600, 800, and 1100 °C and kept at these temperatures for at least 4 hours in air. After the heat treatment was completed, the samples were cooled to ambient temperature together with the furnace. The ceramic material required for the study of the mechanical properties of $MgFeInO_4$ was made from a powder that does not contain impurity phases. Before pressing, it was ground in a mortar, moistened with a few drops of acetone ($\omega(CH_3COCH_3)$ = 99.75 wt. %, National State Standard GOST 2768-84). The resulting mass was transferred to a steel mold, and tablets with a diameter of 14 mm were formed from it, using a manual hydraulic press. The compacted samples were sintered at 1300 °C for 6 hours in air. After its completion, the sintered ceramics were left in the furnace until it cooled completely. The actual density (d_{obs}, kg/m^3) of the samples obtained was determined geometrically. Their relative porosity (p_{rel}, %) was estimated by the formula:

$$p_{rel} = 100\left(1 - \frac{d_{obs}}{d_{XRD}}\right), \quad (1)$$

where d_{XRD} (in kg/m^3) is the theoretical density of ceramics determined from powder X-ray diffraction data.

2.2. Characterization of the obtained materials

The phase composition of the materials obtained was determined using the powder X-ray diffraction (XRD) method on a Bruker D8 Advance diffractometer equipped with the LynxEye linear detector. An X-ray tube with a copper anode ($\lambda(CuK_\alpha)$ = 1.5418 Å) was used as the radiation source. A nickel filter was used to eliminate the CuK_β-radiation. The XRD patterns for all samples studied were recorded at room temperature in the range of angles 2θ = 10 – 60° with a step of 0.0133° and a signal accumulation time of 0.5 s/step. X-ray phase analysis was performed using the ICDD PDF-2 database and Bruker DIFFRAC. EVA software. The calculation of crystallographic parameters and sizes of coherent scattering regions (CSR) was performed using Bruker TOPAS 4.2 software.

The microstructure of the synthesized materials was studied using scanning electron microscopy (SEM). SEM images in the secondary electron detection mode were obtained using an ultra-high-resolution scanning electron microscope TESCAN AMBER. The freely distributed Gwyddion software [33] was used to analyse the obtained SEM data and to plot the particle size distribution curve.

Data on the elemental composition of the synthesized magnesium-indium ferrite was obtained by energy dispersive X-ray spectroscopy (EDS) using an Oxford Instruments Ultim MAX SDD detector.

The study of ceramic microhardness (H) by the Vickers method was carried out on a LOMO PMT-3M microhardness tester. Before measurements, the surface of the samples was washed and polished in an aqueous alcohol solution under ultrasonic treatment. The measurements were conducted with a static load on the indenter equal to 0.49 N (50 g). The duration of the load application was 10 seconds.

The diffuse reflectance spectra $R(\lambda)$ of the samples in the range of 200 – 950 nm were recorded using the Ocean Optics modular optical system, which includes a QE65000 spectrometer, an integrating sphere ISP-80-8-R with a diameter of 80 mm, and a set of optical fibers. The source of the radiation was an HPX-2000 xenon lamp. The Labsphere WS-1-SL standard made of spectralon was used as a reference standard material. The spectrometer was controlled using the Spectra Suite software.

3. Results and discussion

3.1. X-ray phase analysis, composition, and structural and morphological characteristics of synthesized materials

The XRD data for the synthesized precursor powder is shown in Fig. 1. The absence of crystal phase peaks on the diffractogram obtained (curve 1) indicates its X-ray amorphous structure. This result is accounted for the fact that the decomposition of products formed by heating a mixture of solutions of metal nitrates and PVA is not accompanied by combustion (smolder) and is likely to occur at relatively low temperatures [34]. According to [35, 36], this mode of the process contributes to the formation of thermally stable polymer-metal complexes, and their short-term annealing enables one to obtain nanocrystalline powders of complex metal oxides at 500 – 800 °C.

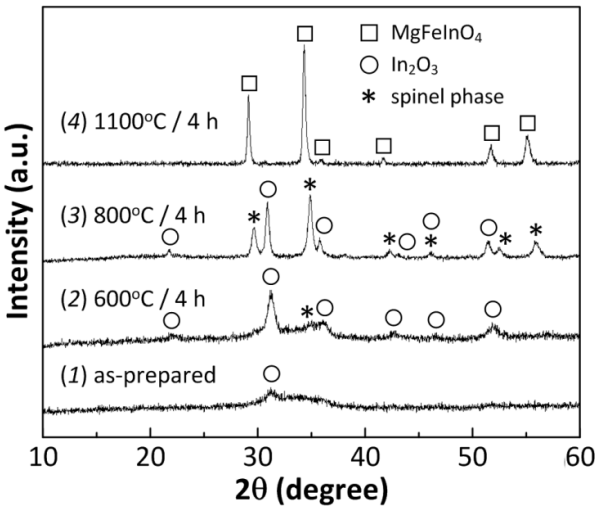

FIG. 1. XRD data for the samples obtained after annealing of precursor powder at different temperatures in air

XRD data for the precursor powder after its heat treatment in air at 600, 800, and 1100 °C are shown in Fig. 1 (curves 2–4). The results obtained show that very wide and low-intensity maxima appear on the diffractogram of the powder annealed at 600 °C (curve 2). According to the X-ray phase analysis, it is a mixture consisting mainly of In_2O_3 (sp. gr. $I\bar{a}3$, PDF card No. 06-0416) and a small amount of $MgFe_{2-x}In_xO_4$ phase with a spinel structure. According to the calculation results, the average crystallite size in this powder is about 10 nm. An attempt to anneal the X-ray amorphous precursor at a higher temperature also failed to produce a single-phase ferrite-spinel sample of the composition required. As can be seen from Fig. 1 (curve 3), the diffractogram of the powder annealed at 800 °C (4 h) shows more intense, wide maxima related to the $MgFe_{2-x}In_xO_4$ phase, but it still contains an admixture of In_2O_3. The amount of ferrite-spinel in this powder reaches about 80 %, and the average size of its crystallites increases to 30 nm. Moreover, as the results of our experiments showed, even a threefold increase in the annealing duration at this temperature does not lead to the production of a single-phase sample of $MgFeInO_4$. It can be obtained only by increasing the annealing temperature to 1100 °C. As can be seen from the diffraction pattern of the annealed powder (Fig. 1, curve 4), all diffraction maxima correspond to $MgFeInO_4$ ferrite-spinel (sp. gr. $Fd\bar{3}m$, PDF card No. 38-1108). The disappearance of the (111) diffraction line indicates a very high degree of its inversion, which tends to 1. This result differs from the data obtained by Matvejeff *et al.* [31] and is explained by the differences in the chemical and thermal prehistory of the $MgFeInO_4$ samples being compared. The parameter a and the unit cell volume V_{cell} of synthesized $MgFeInO_4$ are 8.6391(6) Åand 644.8(1) $Å^3$, respectively, and its X-ray density d_{XRD} is 5336 kg/m^3. Literature data comparison showed that the calculated values are close to those obtained for samples synthesized by the solid-phase method [30, 31].

The data on the chemical composition of the $MgFeInO_4$ sample obtained by the EDS are shown in Fig. 2. It is obvious that the actual content of magnesium, iron, and indium in it (inset in Fig. 2) almost coincides with the theoretical one: ω_{theor}(Mg) = 9.39 wt. %, ω_{theor}(Fe) = 21.56 wt. %, and ω_{theor}(Fe) = 44.34 wt. %. Thus, the chemical composition of the synthesized ferrite-spinel can be represented as $Mg_{1.01\pm0.08}Fe_{0.99\pm0.07}In_{0.99\pm0.06}O_4$.

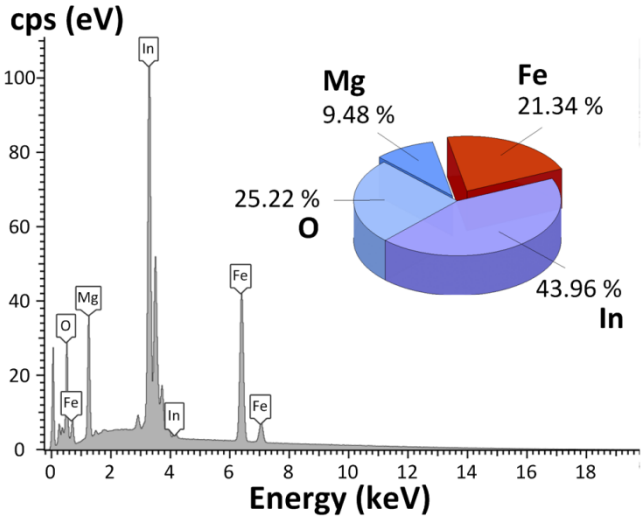

FIG. 2. EDS spectrum of $MgFeInO_4$ synthesized by annealing of precursor powder at 1100 °C for 4 hours. Inset: diagram illustrating the elemental composition of the sample (in wt. %), determined from the EDS data

It is noteworthy that the annealing temperature required to obtain a single-phase $MgFeInO_4$ powder turned out to be significantly higher than that used for the synthesis of $MgFe_2O_4$. A single-phase powder of this spinel was reported to be formed after annealing the precursor at 700 °C [37]. Similar results were obtained in [38], in which it was successfully synthesized by calcination of starch-nitrate gel at 550 °C. At the same time, the sol-gel method used in [32] did not result in obtaining single-phase $MgFe_{2-x}In_xO_4$ nanopowders with $x = 0.16$ at 600 °C. Previously, we showed [39] that single-phase $MgIn_2O_4$ is formed only after annealing of solid-phase combustion products of a glycine-nitrate gel at 1400 °C. Similar observations were made in [40], where this spinel was obtained by long-term high-temperature annealing (1300 °C, 60 h) of a precursor synthesized by the oxalate method. It is remarkable that the difference in annealing temperatures used for the synthesis of $MgFe_{2-x}In_xO_4$ solid solution boundary compositions is more than 700 °C, and the minimum annealing temperature required to obtain a single-phase composition with 50 % substitution of indium cations is about 400 °C higher than for $MgFe_2O_4$. The obtained result can be explained as follows. According to [41], the stable form of magnesium indate occurs only above 1200 °C, and the process of its formation from simple oxides is endothermic in nature. Therefore, the energy spent on breaking bonds in compounds used for spinel synthesis will exceed the energy released during the formation of bonds in it. Thus, the formation of $MgIn_2O_4$ requires additional energy input from the surroundings. Magnesium ferrite, on the contrary, has a negative enthalpy of formation ($\Delta H^0_{f,ox}$(970 K) = -18.5 ± 1.0 kJ/mol [42]). The enthalpy of formation for $MgFeInO_4$ is unknown, but according to our results it can be assumed to be lower than that of $MgIn_2O_4$. Consequently, mixed ferrite can be synthesized at lower temperatures than $MgIn_2O_4$. However, annealing of the precursor powder at high temperatures, as in the case of $MgIn_2O_4$ [39, 40], does not imply the production of single-phase $MgFeInO_4$ nanocrystalline powder. Nevertheless, the width and intensity of the maxima observed on the diffractogram of the powder annealed at 1100 °C (Fig. 1, curve 4) indicate relatively low values of CSRs.

The results of the microscopic study of the changes occurring in the structure and morphology of the particles of the X-ray amorphous precursor as a result of annealing at temperatures ranging from 600 to 1100 °C are presented in Fig. 3(a–c). The microstructure of the nanopowders formed after annealing at 600 and 800 °C (Fig. 3(a) and (b)) exhibits a sponge-like structure, which makes it difficult to distinguish the contours of individual crystallites. As seen in Fig. 3(c), increasing the annealing temperature of the precursor powder to 1100 °C led to the formation of $MgFeInO_4$ particles that are fairly uniform in size, though lacking well-defined faceting. The histogram illustrating their size distribution is shown in Fig. 3(f). The results of fitting these data using a Gaussian distribution function revealed that the average particle size of the ferrite-spinel synthesized is 0.90 μm.

The ceramics obtained by sintering the compacts of $MgFeInO_4$ powder at 1300 °C for 6 hours in air had a bulk density d_{obs} equal to about 4800 kg/m^3. The porosity P_{obs} of the sample produced, calculated using Eq. (1), was about 10 %, which indicates its high density.

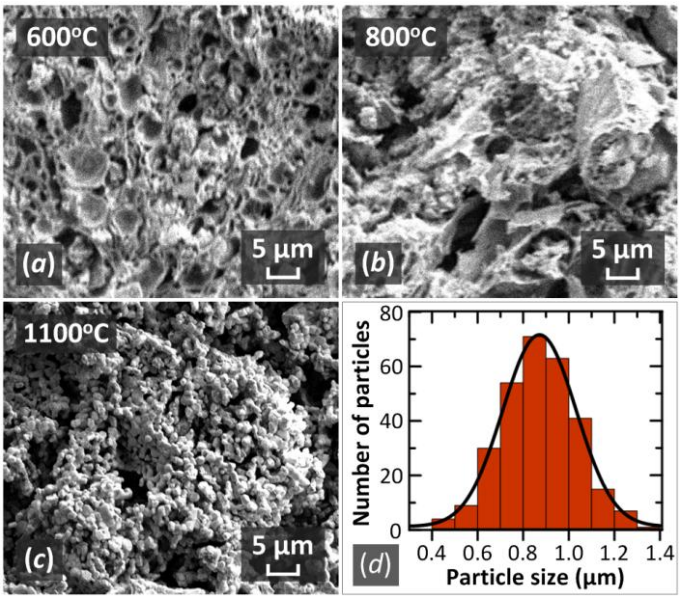

FIG. 3. (a–c) SEM images of powders obtained after annealing the precursor powder at 600 °C (4 h), 800 °C (4 h), and 1100 °C (4 h) in air. (d) Particle size distribution curve for the $MgFeInO_4$ sample obtained after annealing at 1100 °C (4 h)

3.2. Vickers microhardness

No data on the microhardness of $MgFeInO_4$ measured by the Vickers method was found in the literature. Based on the experimental results, the average microhardness value of the produced ceramics was determined to be 676 HV. It may be noted that the obtained value of H is close to those measured for magnetite Fe_3O_4 (610 HV) and manganese ferrite $MnFe_2O_4$ (734 HV) [43]. The hardness class of $MgFeInO_4$ was determined according to the relation proposed in [44]:

$$H_0 = 0.675 \cdot \sqrt[3]{H}, \tag{2}$$

where H_0 is the hardness class of the material on a 15-point scale, in which graphite corresponds to 1 and diamond to 15, and H is the measured Vickers microhardness of the material. According to the recalculation using Eq. (2), the hardness class of the synthesized material on the Khrushchov scale is close to 6. From the viewpoint of the rational classification of materials by hardness proposed in [44], $MgFeInO_4$ belongs to high-hardness materials.

3.3. Band gap energy

Consider the results of diffuse reflectance spectroscopy for the synthesized ferrite-spinel $MgFeInO_4$. A typical dependence of the diffuse reflectance coefficient R on the wavelength of incident light λ is shown in Fig. 4. To calculate the band gap energy E_g, the Tauc method was employed. The $R(\lambda)$ data was presented in the form of the dependence $(F(R) \cdot h\nu)^n$ on $h\nu$, where $F(R)$ is the Kubelka–Munk function, defined as $(1-R)^2/2R$; h is Planck's constant; ν is the frequency of the incident radiation; and n is an exponent characterizing the nature of electron transition in the material. The type of transitions occurring in $MgFeInO_4$ is not precisely known; however, as shown in [38, 45–47], direct allowed transitions dominate in the unsubstituted $MgFe_2O_4$ and $MgIn_2O_4$. Therefore, to determine E_g, coordinates corresponding to the case of direct allowed transitions ($n = 2$) were used. The result of this analysis is shown in the inset of Fig. 4.

Extrapolation of the linear portion of the resulting curve to the abscissa axis at $(F(R) \cdot h\nu)^2 = 0$ yields a band gap energy $E_g = 2.46 \pm 0.02$ eV. The band gap value obtained (2.46 eV) lies between those reported for $MgFe_2O_4$ (2.1 eV [45]) and $MgIn_2O_4$ (3.2 eV) [46], confirming the formation of a solid solution based on these spinels and indicating that the material obtained is a wide-band gap semiconductor.

3.4. Assessment of the radiation tolerance of $MgFeInO_4$

Consider several criteria commonly used to predict the response of solids to high doses of ion impact. Pearton *et al.* [48] reported that the materials with smaller unit cell volumes and wider band gaps tend to be more resistant to ionizing radiation than those with larger cell volumes and narrower band gaps. The values of E_g and V_{cell} for $MgFeInO_4$ and several other spinel-structured materials are summarized in Table 1.

As noted above, Fe_3O_4 is considered one of the most radiation-resistant materials [14]; therefore, its parameters were used as a reference in the analysis of the E_g and V_{cell} data. It is evident that within the series $MgFe_2O_4$ – Fe_3O_4 – $MgFeInO_4$ – $MgIn_2O_4$, both of these parameters increase. Although $MgIn_2O_4$ exhibits the widest band gap among the materials listed, its unit cell volume is 17.7 % larger than that of Fe_3O_4. The E_g and V_{cell} values for $MgFe_2O_4$ and

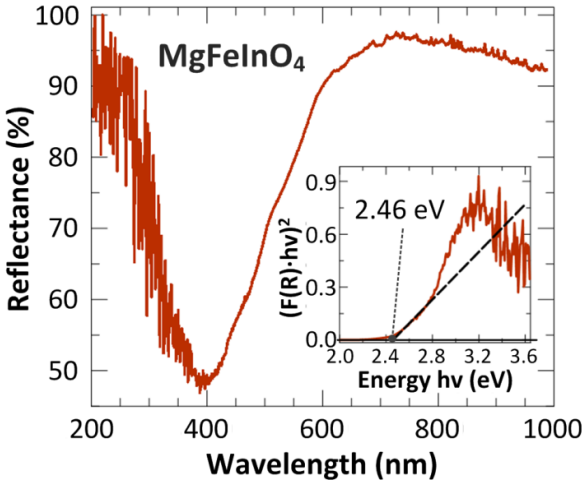

FIG. 4. Diffuse reflectance spectrum of $MgFeInO_4$ measured in the range 200 – 950 nm. Inset: representation of the data as a dependence of $(F(R) \cdot h\nu)^2$ on photon energy $h\nu$

TABLE 1. Physical properties of some spinel-structured materials

Material	Unit cell volume V_{cell}, Å^3	Band gap energy E_g, eV	Ionicity f	Predicted structure following irradiation
$MgFe_2O_4$	589.32 [38]	2.1 [45]	0.57*	–
Fe_3O_4	591.86 [49]	2.29 [50]	0.49*	Crystal [51]
$MgFeInO_4$	644.8*	2.46*	0.58	Crystal**
$MgIn_2O_4$	696.59 [39]	3.2 [46]	0.59*	–

* – determined in this work;

** – predicted structural stability based on the calculated values of ionicity

$MgFeInO_4$ are the closest to those of Fe_3O_4; however, for the mixed ferrite-spinel, the deviation in both parameters does not exceed 9 %. Therefore, materials based on $MgFeInO_4$ are most likely to exhibit radiation resistance comparable to that of Fe_3O_4 under similar irradiation conditions.

Naguib and Kelly [51] showed that the ability of materials to resist radiation damage correlates with the degree of bond ionicity, finding that materials with a more ionic bond character are less susceptible to damage under high doses of ionizing radiation. To put it simply, such materials tend to resist amorphization of the crystal lattice under irradiation. It was also established in [51] that structural changes are likely to occur if the ionicity value f is less than or equal to 0.47. The f values for $MgFe_2O_4$, $MgFeInO_4$, and $MgIn_2O_4$, calculated from the data in [52], are presented in Table 1. For comparison, the f value for Fe_3O_4, determined in [51], is also included. The calculations show that the ionicity in the series $MgFe_2O_4$ – $MgFeInO_4$ – $MgIn_2O_4$ exhibits close values, all significantly exceeding 0.47. Moreover, the ionicity of $MgFeInO_4$ is approximately 18.4 % higher than that of Fe_3O_4, which retains its crystalline structure even under irradiation [14]. Therefore, it can be inferred that magnesium-indium ferrite possesses radiation stability comparable to that of magnetite. Thus, the results of this preliminary assessment indicate the promising potential of $MgFeInO_4$ for further experimental studies on the effects of various ionizing radiation conditions on its structural and physico-mechanical properties.

4. Conclusions

A single-phase powder of the mixed ferrite-spinel $MgFeInO_4$ with submicron particle size was successfully synthesized using the polymer-nitrate method. XRD data obtained for the X-ray amorphous precursor annealed at different temperatures showed that a single-phase ferrite-spinel powder of the desired composition can be synthesized only at 1100 °C. According to SEM data, the average particle size was approximately 0.90 μm. The results obtained indicate that the synthesis of single-phase $MgFeInO_4$ in the nanocrystalline form by the polymer-nitrate method is impossible. However, this approach can be used to produce a compositionally homogeneous submicron ferrite-spinel powder. Moreover, unlike the solid-state method, it requires significantly less time and energy.

The $MgFeInO_4$ powder was used to produce ceramics of the same composition by high-temperature sintering in air. The density measurements showed that the approach applied enables one to obtain a ceramic material with a relative density of at least 90 %. Vickers microhardness testing revealed that the average microhardness value was 676 HV. This corresponds approximately to class 6 on the Khrushchov hardness scale, allowing the material to be classified as hard. The band gap energy value for $MgFeInO_4$ was determined from DRS data. According to the calculation results, the mixed magnesium ferrite can be attributed to wide bandgap materials ($E_g = 2.46$ eV). The electrophysical and structural parameters of $MgFeInO_4$ determined in this work made it possible to predict its ability to resist radiation-induced structural changes. Theoretical analysis showed that this ferrite-spinel is highly likely to retain its crystalline structure under ionizing radiation exposure. This result confirms the potential of further experimental studies on the influence of various irradiation conditions on the structure and functional properties of mixed magnesium-indium ferrites.

References

[1] Orlova A.I., Ojovan M.I. Ceramic mineral waste-forms for nuclear waste immobilization. *Materials*, 2019, **12** (16), 2638.

[2] Kalita P., Parveen R., Ghosh S., Grover V., Mishra Y.K., Avasthi D.K. Progress in radiation tolerant materials: current insights from the perspective of grain size and environmental temperature. *J. of Alloys and Compounds*, 2025, **1012**, 178330.

[3] More C.V., Akman F., Dilsiz K., Ogul H., Pawar P.P. Estimation of neutron and gamma-ray attenuation characteristics of some ferrites: Geant4, FLUKA and WinXCom studies. *Applied Radiation and Isotopes*, 2023, **197**, 110803.

[4] Li Z., Chan S.-K., Garner F.A., Brandt R.C. Elastic stability of high dose neutron irradiated spinel. *J. of Nuclear Materials*, 1995, **219**, P. 139–142.

[5] Wang L., Gong W., Wang S., Ewing R.C. Comparison of ion-beam irradiation effects in X_2YO_4 compounds. *J. of the American Ceramic Society*, 1999, **82** (12), P. 3321–3329.

[6] Pellerin N., Dodane-Thiriet C., Montouillout V., Beauvy M., Massiot D. Cation sublattice disorder induced by swift heavy ions in $MgAl_2O_4$ and $ZnAl_2O_4$ spinels: ^{27}Al Solid-State NMR Study. *The Journal of Physical Chemistry B*, 2007, **111** (44), P. 12707–12714.

[7] Wiss T., Matzke Hj. Heavy ion induced damage in $MgAl_2O_4$, an inert matrix candidate for the transmutation of minor actinides. *Radiation Measurements*, 1999, **31** (1-6), P. 507–514.

[8] Yasuda K., Matsumura S. Radiation damage effects in insulators for fusion reactors: microstructure evolution in MgO-Al_2O_3 system oxide crystals. *Advances in Science and Technology*, 2006, **45**, P. 1961–1968.

[9] Burghartz M., Matzke Hj., Léger C., Vambenepe G., Rome M. Inert matrices for the transmutation of actinides: fabrication, thermal properties and radiation stability of ceramic materials. *J. of Alloys and Compounds*, 1998, **271–273**, P. 544–548.

[10] Neeft E.A.C., Bakker K., Schram R.P.C., Conrad R., Konings R.J.M. The EFTTRA-T3 irradiation experiment on inert matrix fuels. *J. of Nuclear Materials*, 2003, **320** (1–2), P. 106–116.

[11] Kinoshita C., Fukumoto K., Fukuda K., Garner F.A., Hollenberg G.W. Why is magnesia spinel a radiation-resistant material? *J. of Nuclear Materials*, 1995, **219**, P. 143–451.

[12] Pascard H., Studer F. Review of irradiation effects on ferrites: results in the world from 1970 to 1995. *Journal de Physique IV*, 1997, **7** (C1), P. 211–214.

[13] Houpert C., Hervieu M., Groult D., Studer F., Toulemonde M. HREM investigation of GeV heavy ion latent tracks in ferrites. *Nuclear Instruments and Methods in Physics Research Section B: Beam Interactions with Materials and Atoms*, 1988, **32** (1–4), P. 393–396.

[14] Meillon S., Dunstetter F., Pascard H., Rodriguez-Carvajal J. Fast neutron irradiated magnetite and haematite investigated by neutron diffraction. *Journal de Physique IV Proceedings*, 1997, **07** (C1), P. 607–608.

[15] Sickafus K.E., Yu N., Nastasi M. Radiation resistance of the oxide spinel: the role of stoichiometry on damage response. *Nuclear Instruments and Methods in Physics Research Section B: Beam Interactions with Materials and Atoms*, 1996, **116** (1–4), P. 85–91.

[16] Reznitskiy L.A. *Calorimetry of Solids*. Moscow: Mos. Gos. Univ., 1981, 184 p.

[17] Šepelák V., Becker K.D. Comparison of the cation inversion parameter of the nanoscale milled spinel ferrites with that of the quenched bulk materials. *Materials Science and Engineering: A*, 2004, **375–377**, P. 861–864.

[18] Kingery W.D. *Introduction to ceramics, 2nd Edition*. John Wiley & Sons, 1976, 1056 p.

[19] Shen T.D. Radiation tolerance in a nanostructure: Is smaller better? *Nuclear Instruments and Methods in Physics Research B*, 2008, **266** (6), P. 921–925.

[20] Andrievskii R.A. Radiation stability of nanomaterials. *Nanotechnologies in Russia*, 2011, **6**, P. 357–369.

[21] Lokhande R.M., Vinayak V., Mukhamale S.V., Khirade P.P. Gamma radiation shielding characteristics of various spinel ferrite nanocrystals: a combined experimental and theoretical investigation. *RSC Advances*, 2021, **11** (14), P. 7925–7937.

[22] Satalkar M., Kane S.N., Kulriya P.K., Avasthi D.K. Swift heavy ion irradiated spinel ferrite: A cheap radiation resistant material. *Nuclear Instruments and Methods in Physics Research Section B: Beam Interactions with Materials and Atoms*, 2016, **379**, P. 235–241.

[23] Sharma S.K., Kumar R., Siva Kumar V.V., Knobel M., Reddy V.R., Gupta A., Singh. M. Role of electronic energy loss on the magnetic properties of $Mg_{0.95}Mn_{0.05}Fe_2O_4$ nanoparticles, *Nuclear Instruments and Methods in Physics Research Section B: Beam Interactions with Materials and Atoms*, 2006, **248** (1), P. 37–41.

[24] Parvatheeswara Rao B., Rao K.H., Subba Rao P.S.V., Mahesh Kumar A., Murthy Y.L.N., Asokan K., Siva Kumar V.V., Kumar R., Gajbhiye N.S., Caltun O.F. Swift heavy ions irradiation studies on some ferrite nanoparticles. *Nuclear Instruments and Methods in Physics Research Section B: Beam Interactions with Materials and Atoms*, 2006, **244** (1), P. 27–30.

[25] Hassan H.E., Sharshar T., Hessien M.M., Hemeda O.M. Effect of γ-rays irradiation on Mn–Ni ferrites: Structure, magnetic properties and positron annihilation studies. *Nuclear Instruments and Methods in Physics Research Section B: Beam Interactions with Materials and Atoms*, 2013, **304**, P. 72–79.

[26] Jagadeesha Angadi V., Anupama A.V., Choudhary H.K., Kumar R., Somashekarappa H.M., Mallappa M., Rudraswamy B., Sahoo B. Mechanism of γ-irradiation induced phase transformations in nanocrystalline $Mn_{0.5}Zn_{0.5}Fe_2O_4$ ceramics. *J. of Solid State Chemistry*, 2017, **246**, P. 119–124.

[27] Chikhale R.N., Shinde V.S., Bhatia P.G. Investigate structural, morphological, electrical, dielectric and magnetic properties of dysprosium doped cobalt-nickel ferrites and their response to gamma irradiation. *Nuclear Instruments and Methods in Physics Research Section B: Beam Interactions with Materials and Atoms*, 2024, **550**, 165320.

[28] Manjunatha, Biradar S., Bennal A.S., Patil S., Sayyed M.I., Patil Y.N., Megalamani M.B., Hegde B.G. Experimental investigation on the role of Bi^{3+} composition in structural, elastic, and radiation shielding properties of multifunctional cobalt-nickel nanoferrites. *J. of Alloys and Compounds*, 2025, **1033**, 181255.

[29] Kirichok P.P., Antoshchuk, Mössbauer investigations into magnesium ferrite doped with indium and scandium ions. *Soviet Physics Journal*, 1977, **20**, P. 627–630.
[30] Kimizuka N., Mohri T. Spinel, $YbFe_2O_4$, and $Yb_2Fe_3O_7$ types of structures for compounds in the In_2O_3 and Sc_2O_3–A_2O_3–BO systems [A: Fe, Ga, or Al; B: Mg, Mn, Fe, Ni, Cu, or Zn] at temperatures over 1000°C. *J. of Solid State Chemistry*. 1985, **60**, P. 382–384.
[31] Matvejeff M., Lindén J., Karppinen M., Yamauchi H. Studies on $InFeMO_4$ (M = Mg, Co, Ni, Cu and Zn) compounds: crystal structure and cation distribution. *Journal of Solid State Chemistry*, 2007, **180** (8), P. 2316–2322.
[32] Naik M.Z., Salker A.V. Tailoring the super-paramagnetic nature of $MgFe_2O_4$ nanoparticles by In^{3+} incorporation. *Materials Science and Engineering B*, 2016, **211**, P. 37–44.
[33] Necas D., Klapetek P. Gwyddion: an open-source software for SPM data analysis. *Open Physics*, 2012, **10** (1), P. 181–188.
[34] Khaliullin Sh.M., Zhuravlev V.D., Bamburov V.G., Khort A.A., Roslyakov S.I., Trusov G.V., Moskovskikh D.O. Effect of the residual water content in gels on solution combustion synthesis temperature. *Journal of Sol-Gel Science and Technology*, 2020, **93**, P. 251–261.
[35] Kondratéva O.N., Smirnova M.N., Nikiforova G.E., Yapryntsev A.D., Kondakov D.F., Yagudin L.D. Ceramic materials prepared from nanocrystalline $InFeZnO_4$ powder: optical and mechanical properties, and evaluation of radiation tolerance. *Nanosystems: Physics, Chemistry, Mathematics*, 2024, **15** (5), P. 693–701.
[36] Smirnova M.N., Kondrat'eva O.N., Nikiforova G.E., Yapryntsev A.D., Averin A.A., Khoroshilov A.V. Features of synthesis of $InGaMgO_4$ from nitrate-organic precursors and study of its physical properties. *Russian J. of Inorganic Chemistry*, 2024, **69**, P. 1119–1126.
[37] Smirnova M.N., Nikiforova G.E., Kondrat'eva O.N. Synthesis of magnesium ferrite by combustion of glycine-nitrate gel: the influence of reagents on the gel-precursor and the microstructure of nanopowders, *Nanosystems: Physics, Chemistry, Mathematics*, 2024, **15** (2), P. 224–232.
[38] Köferstein R., Walther T., Hesse D., Ebbinghaus S.G. Preparation and characterization of nanosized magnesium ferrite powders by a starch-gel process and corresponding ceramics. *J. of Materials Science*, 2013, **48**, P. 6509–6518.
[39] Kondrat'eva O.N., Smirnova M.N., Nikiforova G.E., Khoroshilov A.V., Arkhipenko A.A., Gurevich V.M. Magnesium indate: synthesis and thermodynamic properties. *Russian J. of Inorganic Chemistry*, 2022, **67**, P. 1221–1227.
[40] Jayachandran M., Dali S.E., Chockalingam M.J. Synthesis and characterisation of semiconductor oxide $MgIn_2O_4$ powder. *Bulletin of Electrochemistry*, 1998, **14** (8–9), P. 283–285.
[41] Pokrovskii B.I., Gapeev A.K., Goryaga A.N., Komissarova L.N. *Crystal chemistry and magnetism of mixed gallium- and indium-containing ferrites with spinel structure. Ferrimagnetism*. Moscow: Mos. Gos. Univ., 1975, P. 137–146.
[42] Navrotsky A., Kleppa O.J. Thermodynamics of formation of simple spinels. *J. of Inorganic and Nuclear Chemistry*, 1968, **30** (2), P. 479–498.
[43] Lebedeva S.I. *Determination of Microhardness of Minerals*. Moscow: Publishing house of the USSR Academy of Sciences, 1963, 124 p.
[44] Khrushchev M.M. *Friction, Wear and Microhardness of Materials: Selected Works*. Moscow: KRASAND, 2012, 512 p.
[45] Anagha A., Joshua A., Chacko B., Babu T.A., Srigiri S., Madhuri W. Structural, optical and magnetic properties of $MgFe_2O_4$ and $Ni_{0.5}Zn_{0.5}Fe_2O_4$. *Materials Chemistry and Physics*, 2024, **313**, 128746.
[46] Sirimanne P.M., Sonoyama N., Sakata T. Semiconductor sensitization by microcrystals of $MgIn_2S_4$ on wide bandgap $MgIn_2O_4$. *Journal of Solid State Chemistry*, 2000, **154** (2), P. 476–482.
[47] Ueda N., Hosono H., Kawazoe H. Noble transparent semiconductor: $MgIn_2O_4$. *Solid State Phenomena*, 1996, **51–52**, P. 317–322.
[48] Pearton S.J., Yang J., Cary P.H., Ren F., Kim J., Tadjer M.J., Mastro M.A. A review of Ga_2O_3 materials, processing, and devices. *Applied Physics Review*, 2018, **5** (1), 011301.
[49] Geng H., Zhou Q., Zheng J., Gu H. Preparation of porous and hollow Fe_3O_4@C spheres as an efficient anode material for a high performance Li-ion battery. *RSC Advances*, 2014, **4** (13), P. 6430–6434.
[50] da Silva M.P., do Souza A.C.A., Ferreira Á.R.D., do Nascimento P.L.A., Fraga T.J.M., Cavalcanti J.V.F.L., Ghislandi M.G., da Motta Sobrinho M. A. Synthesis of superparamagnetic Fe_3O_4–graphene oxide-based material for the photodegradation of clonazepam, Scientific Reports, 2024, **14**, 18916.
[51] Naguib H.M., Kelly R. Criteria for bombardment-induced structural changes in non-metallic solids. *Radiation Effects*, 1975, **25** (1), P. 1–12.
[52] Batsanov S.S. The concept of electronegativity. Conclusions and prospects. *Russian Chemical Reviews*, 1968, **37** (5), P. 332–351.

Submitted 14 November 2025; revised 30 November 2025; accepted 2 December 2025

Information about the authors:

Olga N. Kondrat'eva – Kurnakov Institute of General and Inorganic Chemistry of the Russian Academy of Sciences, Leninskii prosp., 31, Moscow, 119991, Russia; ORCID 0000-0003-2508-9868; ol.kondratieva@gmail.com

Maria N. Smirnova – Kurnakov Institute of General and Inorganic Chemistry of the Russian Academy of Sciences, Leninskii prosp., 31, Moscow, 119991, Russia; ORCID 0000-0003-2707-7975; smirnovamn@igic.ras.ru

Galina E. Nikiforova – Kurnakov Institute of General and Inorganic Chemistry of the Russian Academy of Sciences, Leninskii prosp., 31, Moscow, 119991, Russia; ORCID 0000-0002-2892-6054; gen@igic.ras.ru

Alexey D. Yapryntsev – Kurnakov Institute of General and Inorganic Chemistry of the Russian Academy of Sciences, Leninskii prosp., 31, Moscow, 119991, Russia; ORCID 0000-0001-8166-2476; yaprynsev@yandex.ru

Maria S. Dranik – Frumkin Institute of Physical Chemistry and Electrochemistry of the Russian Academy of Sciences, Leninskii prosp., 31.4, Moscow, 119071, Russia; ORCID 0009-0006-1953-2359; m.dranik@yandex.ru

Valery A. Ketsko – Kurnakov Institute of General and Inorganic Chemistry of the Russian Academy of Sciences, Leninskii prosp., 31, Moscow, 119991, Russia; ORCID 0000-0002-2075-1755; ketsko@igic.ras.ru

Conflict of interest: the authors declare no conflict of interest.